International Journal of Bifurcation and Chaos, Vol. 22, No. 9 (2012) 1250219 (9 pages)

DOI: 10.1142/S0218127412502197

EFFICIENT CONTROL OF ACCELERATOR MAPS

JEHAN BOREUX* and TIMOTEO CARLETTI†
Namur Center for Complex Systems, naXys,
University of Namur, Rempart de la Vierge 8,
Namur 5000, Belgium
**jehan.boreux@fundp.ac.be*
†*timoteo.carletti@fundp.ac.be*

CHARALAMPOS SKOKOS
Max Planck Institute for the Physics of Complex Systems,
Nöthnitzer Str. 38, D-01187 Dresden, Germany

Center for Research and Applications of Nonlinear Systems,
University of Patras, GR-26500 Patras, Greece
hskokos@pks.mpg.de

YANNIS PAPAPHILIPPOU
CERN, CH-1211 Geneva 23, Switzerland
yannis@cern.ch

MICHEL VITTOT
Centre de Physique Théorique,
Aix-Marseille Universite, CNRS-UMR 7332, USTV,
FRUMAM F-13288 Marseille, cedex 9, France
vittot@cpt.univ-mrs.fr

Received March 29, 2011

Recently, the Hamiltonian Control Theory was used in [Boreux *et al.*, 2012] to increase the dynamic aperture of a ring particle accelerator having a localized thin sextupole magnet. In this paper, these results are extended by proving that a simplified version of the obtained general control term leads to significant improvements of the dynamic aperture of the uncontrolled model. In addition, the dynamics of flat beams based on the same accelerator model can be significantly improved by a reduced controlled term applied in only one degree of freedom.

Keywords: Hamiltonian control; particle accelerators; dynamical aperture; symplectic maps; SALI method.

1. Introduction

Hamiltonian Control Theory has been developed in [Vittot, 2004; Chandre *et al.*, 2005] aiming to improve some selected features of a given Hamiltonian system (like to reduce its chaotic behavior), by adding a "small control term" which slightly alters the Hamiltonian of the system.

This technique was adapted in [Boreux *et al.*, 2012] to the case of symplectic maps. In particular, it was applied to a four-dimensional (4D) map which models a simplified accelerator ring with sextupole nonlinearity, succeeding to increase the stability domain around the nominal circular orbit (the so-called dynamic aperture — DA). This procedure allowed the construction of a sequence of control terms of increasing complexity, that successively improve the dynamics of the original map. Actually, the larger the DA became, the functional

complexity of the control term increased, and the required CPU time for the evolution of orbits grew. Real accelerators are composed of such simplified maps (see for example [Forest, 1998]). Thus, we believe that the study of these maps can guide the research for increasing the DA of more complicated models.

The aim of the present paper is to show that simplified versions of the general control term can also lead to a significant increase of the DA. For accelerators, the addition of a control term can be interpreted as the addition of an extra magnet. Since magnetic fields depend only on spatial variables we investigate the efficiency of a modified control term obtained by neglecting the dependence on the momenta of the general control term constructed in [Boreux *et al.*, 2012].

In many real accelerators, the vertical extent of the beam is much smaller than its horizontal size. Such cases can be approximated by considering ideal, flat beams of zero height, whose dynamics is described by a restriction of the general 4D accelerator model to a two-dimensional subspace. We also apply our control theory to a 2D map model of this type, improving the stability of the flat beam.

2. The Model of a Simplified Accelerator Ring

As in [Bountis & Tompaidis, 1991; Bountis & Skokos, 2006a; Boreux *et al.*, 2012] we consider a simplified accelerator ring with linear frequencies (tunes) q_x, q_y, having a localized thin sextupole magnet. The evolution of a charged particle is modeled by the 4D symplectic map

$$\begin{pmatrix} x_1' \\ x_2' \\ x_3' \\ x_4' \end{pmatrix} = \begin{pmatrix} \cos\omega_1 & -\sin\omega_1 & 0 & 0 \\ \sin\omega_1 & \cos\omega_1 & 0 & 0 \\ 0 & 0 & \cos\omega_2 & -\sin\omega_2 \\ 0 & 0 & \sin\omega_2 & \cos\omega_2 \end{pmatrix} \begin{pmatrix} x_1 \\ x_2 + x_1^2 - x_3^2 \\ x_3 \\ x_4 - 2x_1x_3 \end{pmatrix} = T_S \begin{pmatrix} x_1 \\ x_2 \\ x_3 \\ x_4 \end{pmatrix}. \quad (1)$$

where x_1 (x_3) denotes the initial deflection from the ideal circular orbit in the horizontal (vertical) direction before the particle enters the element, and x_2 (x_4) is the associated momentum. Primes denote positions and momenta after one turn in the ring. The parameters ω_1 and ω_2 are related to the accelerator's tunes q_x and q_y by $\omega_1 = 2\pi q_x$ and $\omega_2 = 2\pi q_y$. In our study, we set $q_x = 0.61803$ and $q_y = 0.4152$ corresponding to a regular orbit as shown in [Vrahatis *et al.*, 1997].[1] The particle dynamics at the nth turn, can be described by the sequence $(x_1(n), x_2(n), x_3(n), x_4(n))_{n\geq 0}$, where the $(n+1)$th positions and momenta are defined as a function of the nth ones by (1).

3. Theoretical Considerations and Numerical Techniques

For sake of completeness, let us briefly recall the theoretical framework developed in [Boreux *et al.*, 2012]. Map (1) naturally decomposes in a integrable part, the rotation by angles ω_1, ω_2 in the planes x_1, x_2 and x_3, x_4 respectively, and a quadratic "perturbation", and can be obtained as the time-1 flow of the following Hamiltonian systems

$$\begin{aligned} H(x_1, x_2, x_3, x_4) &= -\omega_1 \frac{x_1^2 + x_2^2}{2} \\ &\quad - \omega_2 \frac{x_3^2 + x_4^2}{2} \quad \text{and} \\ V(x_1, x_2, x_3, x_4) &= -\frac{x_1^3}{3} + x_1 x_3^2. \end{aligned} \quad (2)$$

Using the notation of the Poisson bracket — which is defined by $\{H\}f := \{H, f\} = \sum_j \frac{\partial H}{\partial p_j}\frac{\partial f}{\partial q_j} - \frac{\partial H}{\partial q_j}\frac{\partial f}{\partial p_j}$ for any function $f(p, q)$ — map (1) can be written as

$$\mathbf{x}' = T_S(\mathbf{x}) = e^{\{H\}} e^{\{V\}} \mathbf{x}, \quad (3)$$

where $\mathbf{x} = (x_1, x_2, x_3, x_4)^{\mathrm{T}} \in \mathbb{R}^4$, $(^{\mathrm{T}})$ denotes the transpose of a matrix, and the exponential map is defined as $e^{\{H\}} f = \sum_{n\geq 0} \frac{\{H\}^n}{n!} f$, with $\{H\}^n f = \{H\}^{n-1}(\{H\}f)$.

[1] We remark that in the theory we developed q_x and q_y have been considered as parameters. So, our results can be straightforwardly applied to other cases, remaining valid for tunes satisfying a nonresonant condition (see Sec. 3). We also note that our method can be easily adapted to the resonant case, but the construction of a new control term is required.

Assuming that the perturbation V is small close to the origin, so that $V = o(H)$, we can construct a *control map* whose generator F is small with respect to V (i.e. it satisfies $F = o(V)$). Moreover, the *controlled map*

$$T_{\rm ctrl} = e^{\{H\}} e^{\{V\}} e^{\{F\}}, \tag{4}$$

is symplectic and conjugated to a map T_*, closer to $e^{\{H\}}$ than T_S (for more details the reader is referred to [Boreux *et al.*, 2012]). Assuming furthermore, that a nonresonant condition is satisfied for the particular choice of the q_x and q_y values of map (1), the generator F of the control map $e^{\{F\}}$ is

$$F = \frac{1}{2}\{V\}\mathcal{G}V + o(V^2), \tag{5}$$

where $\mathcal{G}$ is a "pseudo-inverse" operator, which satisfies $\mathcal{G}(1 - e^{-\mathcal{H}})\mathcal{G} = \mathcal{G}$ (see [Chandre *et al.*, 2005] for more details).

Even truncating the generator F at order two and using

$$F_2 = \frac{1}{2}\{V\}\mathcal{G}V, \tag{6}$$

as an *approximate generator*, the control map $e^{\{F_2\}}$ cannot, in general, be written in a closed analytic form. So, we define a *truncated control map of order k*

$$C_k(F_2) = \sum_{l=0}^{k} \frac{\{F_2\}^l}{l!}, \tag{7}$$

and a *truncated controlled map of order k*:

$$T_k(F_2) = e^{\{H\}} e^{\{V\}} C_k(F_2) = T_S C_k(F_2). \tag{8}$$

Following [Boreux *et al.*, 2012], the Smaller Alignment Index (SALI) method of chaos detection is used to determine the regular or chaotic nature of orbits of map (1) and its controlled version (4). We note that an orbit is considered to escape and collide with the accelerator's vacuum chamber if at some time n $\sum_{i=1}^{4} x_i^2(n) > 10$. For the evaluation of SALI, the tangent of the studied map is computed and employed for following the evolution of two initially linearly independent unit deviation vectors $\hat{v}_1(0)$ and $\hat{v}_2(0)$, defining the index as

$$\begin{aligned} \text{SALI}(n) = \min\{&\|\hat{v}_1(n) + \hat{v}_2(n)\|, \\ &\|\hat{v}_1(n) - \hat{v}_2(n)\|\}, \end{aligned} \tag{9}$$

where $\|\cdot\|$ denotes the usual Euclidean norm and $\hat{v}_i(n) = \frac{\mathbf{v}_i(n)}{\|\mathbf{v}_i(n)\|}$, $i = 1, 2$ are vectors of unit norm.

The behavior of SALI, and its generalization, the so-called Generalized Alignment Index (GALI), has been studied in detail in [Skokos, 2001; Skokos *et al.*, 2003, 2004, 2007]. According to these studies, in 4D maps the SALI of chaotic orbits tends exponentially to zero as $\text{SALI}(n) \propto e^{-(\sigma_1 - \sigma_2)n}$ (with σ_1, σ_2 being the two largest Lyapunov characteristic exponents of the orbit), while it fluctuates around positive values, i.e. $\text{SALI}(n) \propto$ const, for regular orbits. In the case of 2D maps, the SALI tends to zero both for regular and chaotic orbits, as $\text{SALI}(n) \propto 1/n^2$ and $\text{SALI}(n) \propto e^{-\sigma_1 n}$, respectively. Thus, the completely different behaviors of SALI for regular and chaotic orbits allow us to clearly distinguish between the two cases both for 4D and 2D maps.

In the following, we consider an orbit to be chaotic if $\text{SALI}(n) \leq 10^{-8}$ after n iterations. We note that in our studies we typically have $\text{SALI}(n) \gtrsim 10^{-2}$ for regular orbits. Consequently the chosen threshold value ($\text{SALI}(n) \leq 10^{-8}$) safely guarantees the chaotic nature of orbits.

4. The Controlled 4D Map

In [Boreux *et al.*, 2012] it was shown that the fourth order controlled map $T_4(F_2)$, is a very good choice for the controlled system, since it succeeded to considerably increase the DA of the accelerator, keeping also the required CPU time for the evolution of large sets of initial conditions, at acceptable levels.

The computed generator F_2 is a complicated function of both the positions x_1, x_3 and the momenta x_2, x_4 of map (1), and its specific expression is given in the Appendix of [Boreux *et al.*, 2012].

A simple approach for investigating the global dynamics of 4D accelerator maps, used in [Bountis & Skokos, 2006a; Boreux *et al.*, 2012], was the computation of the maximal radius of a four-dimensional hypersphere centered at $(x_1, x_2, x_3, x_4) = (0, 0, 0, 0)$, containing only regular orbits up to a finite but large number of iterations. This approach provides a reliable indication of the size of the DA. Application of this methodology in [Boreux *et al.*, 2012] showed that the controlled map $T_4(F_2)$ has better stability properties than the uncontrolled map (1). Nevertheless, one should keep in mind that the center of these hyperspheres does not bear any

particular physical meaning, as it does not correspond to an experimentally realizable beam configuration.

From a physical point of view, it is more meaningful to study the dynamics of the nominal orbit having $x_1(0) = x_3(0) = 0$ for different momenta x_2, x_4. For this purpose, we consider four-dimensional hyperspheres, centered at $(0, x_2, 0, x_4)$ and compute for different values of x_2, x_4, the radius R of the largest hypersphere which contains only regular orbits.

The outcome of this investigation is presented in Fig. 1, where the x_2, x_4 coordinates of the centers of the considered hyperspheres are colored according to the value of radius R for the uncontrolled map (1) [Fig. 1(a)], and the $T_4(F_2)$ map [Fig. 1(b)]. For both maps, the largest value of R is obtained for $x_2 = x_4 = 0$ (i.e. the value obtained in [Boreux *et al.*, 2012]), while R decreases as the hypershere's center is moved away from $x_2 = x_4 = 0$. This implies that large values of the momenta introduce instabilities and chaotic behavior, which reduce the size of the stability domain.

Nevertheless, the controlled map $T_4(F_2)$ succeeded to increase the stability region, since $R > 0$ for larger values of x_2 and x_4, with respect to the original map. In addition, R attains larger values in the central region of the (x_2, x_4) plane for the controlled map $T_4(F_2)$, being $R \approx 0.6$, which suggests a significant increase of the stability domain around the nominal orbit of the accelerator.

As it has already been mentioned, the controlled map $T_4(F_2)$ has a complicated functional form, depending both on spatial variables x_1, x_3 and on the conjugate momenta x_2, x_4. From a practical point of view, the addition of a control map (7) can be thought as the addition of an appropriate magnetic element in the ring. On the other hand, the vector potential of a Maxwellian magnetic field which is transverse to the particle motion (i.e. without any longitudinal dependence) is a function of these transverse positions and not momenta. It is legitimate then to investigate the efficiency of a modified control term, obtained by neglecting the dependence of F_2 on momenta. In practice, this means that we set $x_2 = x_4 = 0$ in the expression of F_2 obtained in [Boreux *et al.*, 2012], getting

$$\begin{aligned} F_2^{(0)}(x_1, x_3) &:= F_2(x_1, 0, x_3, 0) \\ &= \frac{1}{2}(x_1^2 - x_3^2)\left\{-\frac{1}{6}\csc\left(\frac{3\omega_1}{2}\right)\cos\left(\frac{\omega_1}{2}\right)\right. \\ &\quad \times [x_1^2 - 3x_3^2 + (2x_1^2 - 6x_3^2)\cos(\omega_1)] \\ &\quad + \frac{1}{6}\csc\left(\frac{3\omega_1}{2}\right) x_1^2 \sin\left(\frac{\omega_1}{2}\right)\sin(\omega_1) \\ &\quad \left. - \frac{1}{4}\frac{x_3^2\sin(\omega_2)}{\cos(\omega_2) - \cos(\omega_1 + \omega_2)}\right\} \\ &\quad + \frac{1}{2}\frac{x_1^2 x_3^2 \sin(\omega_2)}{\cos(\omega_2) - \cos(\omega_1 + \omega_2)}. \end{aligned} \tag{10}$$

This is a fourth order polynomial in the positions which may be transformed with some variable rescaling to the vector potential of an octupole magnet with normal symmetry [Wiedemann, 2007]

$$V_{\text{oct}} = b_4 \text{Re}[(x_1 + ix_3)^4], \tag{11}$$

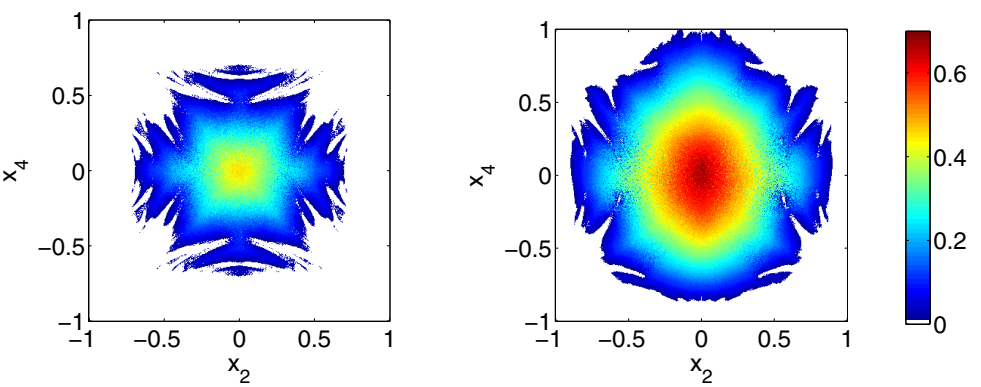

(a) (b)

Fig. 1. The x_2, x_4 coordinates of the centers $(0, x_2, 0, x_4)$ of the four-dimensional hyperspheres containing only regular orbits for (a) the uncontrolled map (1), and (b) the $T_4(F_2)$ map. Each point is colored according to the value of the hypersphere of radius R (with white color corresponding to $R = 0$), and all orbits are evolved up to 10^4 iterations.

where b_4 denotes the multipole coefficient related to the magnet field strength. Since $F_2^{(0)}$ does not depend on the momenta, the control map $e^{\{F_2^{(0)}\}}$, can be explicitly computed. The action of this map on x_2 is given by

$$e^{\{F_2^{(0)}\}}x_2 = x_2 + \{F_2^{(0)}\}x_2 + \frac{\{F_2^{(0)}\}^2}{2!}x_2 + \cdots$$
$$= x_2 - \frac{\partial F_2^{(0)}}{\partial x_1}, \quad (12)$$

because $\{F_2^{(0)}\}x_2$ does not depend on the momenta and consequently $\{F_2^{(0)}\}^m x_2 = 0$ for all integers $m \geq 2$. Similar relations hold also for the other variables, i.e. $\{F_2^{(0)}\}^m x_4 = 0$ for all integers $m \geq 2$ and $\{F_2^{(0)}\}x_1 = \{F_2^{(0)}\}x_3 = 0$. Thus, no truncation of the form (7) is needed, and consequently the simplified controlled map

$$T_C^{(0)} = e^{\{H\}}e^{\{V\}}e^{\{F_2^{(0)}\}}, \quad (13)$$

is symplectic by construction, as a composition of three explicitly known symplectic maps.

Since map $T_C^{(0)}$ is not explicitly constructed by the Hamiltonian Control Theory, it is interesting to check its performance in controlling map (1) and increasing its DA. Following [Bountis & Skokos, 2006a; Boreux *et al.*, 2012], the SALI method is used to determine the regular or chaotic nature of orbits of map $T_C^{(0)}$. In order to directly compare these results with the ones obtained in previous studies, the values of $\log_{10}$ SALI after 10^5 iterations are plotted in Fig. 2, to describe the dynamics in the two-dimensional subspace $x_2(0) = x_4(0) = 0$, for the uncontrolled map (1) [Fig. 2(a)], the $T_4(F_2)$ controlled map (8) [Fig. 2(b)], and the simplified map $T_C^{(0)}$ (13) [Fig. 2(c)]. Chaotic orbits are characterized by small SALI values and are located in the blue colored domains, regular orbits are colored red, while white regions correspond to orbits that escape in less than 10^5 iterations. Figure 2 shows that both controlled maps, $T_4(F_2)$ and $T_C^{(0)}$, increase the DA of the accelerator. It is remarkable that the simplified controlled map $T_C^{(0)}$ not only increases the region of nonescaping orbits, with respect to the original system, but also decreases drastically the number of chaotic orbits.

In order to perform a more global investigation of the dynamics of these maps we consider, as was done in [Bountis & Skokos, 2006a; Boreux *et al.*, 2012], initial conditions inside a four-dimensional hypersphere centered at $x_1 = x_2 = x_3 = x_4 = 0$, and compute the percentages of regular and chaotic orbits as a function of the hypersphere radius r (Fig. 3). From the red curves in Fig. 3, it is observed that the $T_C^{(0)}$ map significantly increases the domain of regular motion, not only with respect to the original map (black curves in Fig. 3), but also with respect to the controlled map $T_4(F_2)$ (blue curves in Fig. 3). In addition, map $T_C^{(0)}$ has the smallest percentage of chaotic orbits among the studied models, which means that orbits of this map either escape or they are regular.

Thus, map $T_C^{(0)}$ (13) controls the original system (1) more efficiently than map $T_4(F_2)$ (8). Additional advantages of this map is its simplicity, since it depends only on the spatial variables, and the fact that it is symplectic by construction. Another

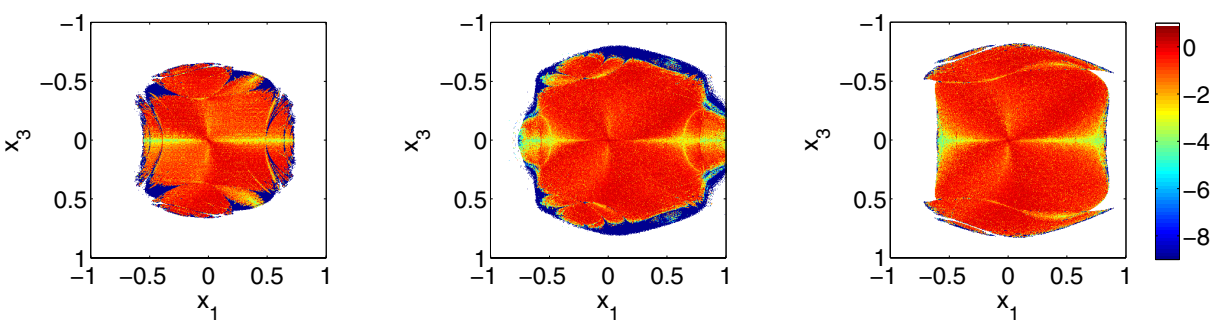

(a) (b) (c)

Fig. 2. Regions of different SALI values on the (x_1, x_3) plane of (a) the uncontrolled map (1), (b) the $T_4(F_2)$ controlled map (8), and (c) the $T_C^{(0)}$ simplified controlled map (13). 16 000 uniformly distributed initial conditions in the square $(x_1, x_3) \in [-1, 1] \times [-1, 1]$, $x_2(0) = x_4(0) = 0$ are followed for 10^5 iterations, and they are colored according to their final $\log_{10}$ SALI value. The white colored regions correspond to orbits that escape in less than 10^5 iterations.

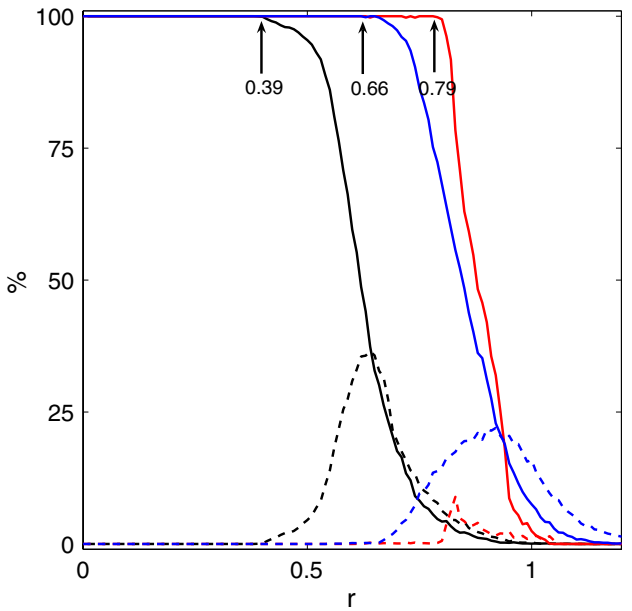

Fig. 3. The percentages of regular (solid curves) and chaotic (dashed curves) orbits after $n = 10^5$ iterations of the original map (1) (black curves), the $T_4(F_2)$ controlled map (8) (blue curves), and the $T_C^{(0)}$ simplified controlled map (13) (red curves), in a four-dimensional hypersphere centered at $x_1 = x_2 = x_3 = x_4 = 0$, as a function of the hypersphere radius r. The largest radii at which the percentage of regular orbits is 100%, are also marked.

feature, which could be of major practical importance, is that the generator $F_2^{(0)}$ (10) of the simplified control map $T_C^{(0)}$ can be considered as the potential induced by a magnetic element, since it depends only on spatial variables.

These results show that the simplified controlled map $T_C^{(0)}$ works better than the controlled map $T_4(F_2)$ which is also able to enlarge the DA with respect to T_S. Then, a natural task would be to compare $T_C^{(0)}$ with $T_{\rm ctrl}$ or with $T_\infty(F_2)$. We note that we were not able to find a closed analytic form for the latter maps due to the cumbersome involved summations. Thus, these comparisons remain open problems which we plan to address in the future. However, we remark that the finite number of terms involved in $T_4(F_2)$ possibly allows the attribution of a real magnetic element to this map, while probably this will not be feasible for maps $T_{\rm ctrl}$ and $T_\infty(F_2)$.

5. Flat Beams: The Controlled 2D Map

In many particle accelerators the beam is very flat, i.e. its vertical extent is much smaller than the horizontal one. A simple, first, approach in investigating the dynamics of a flat beam of the 4D map (1) is to neglect the vertical coordinate x_3 and its corresponding momentum x_4, and pass from the initial 4D map to the 2D map

$$\begin{pmatrix} x_1' \\ x_2' \end{pmatrix} = \begin{pmatrix} \cos\omega_1 & -\sin\omega_1 \\ \sin\omega_1 & \cos\omega_1 \end{pmatrix} \begin{pmatrix} x_1 \\ x_2 + x_1^2 \end{pmatrix} =: T^{\rm 2D} \begin{pmatrix} x_1 \\ x_2 \end{pmatrix}, \quad (14)$$

whose dynamics was studied for example in [Bountis & Skokos, 2006b].

Following for this map, the procedure described in Sec. 3, truncated control $C_k^{\rm 2D}(F_2^{\rm 2D})$ and controlled $T_k^{\rm 2D}(F_2^{\rm 2D})$ maps of order k are constructed, in analogy to Eqs. (7) and (8), respectively. As before, the controlled map is not necessarily symplectic. Since a map is symplectic if its Jacobian matrix $\mathbf{A}$ satisfies (in its definition domain) the equality $\mathbf{A}^{\rm T}\mathbf{J}\mathbf{A} - \mathbf{J} = \mathbf{0}$ (with $\mathbf{J} = \left(\begin{smallmatrix} 0 & 1 \\ -1 & 0 \end{smallmatrix}\right)$ being the standard symplectic constant matrix), the symplectic nature of $T_k^{\rm 2D}(F_2^{\rm 2D})$ can be checked by computing the norm D_k of $\mathbf{A}_k^{\rm T}\mathbf{J}\mathbf{A}_k - \mathbf{J}$, for the Jacobian matrix $\mathbf{A}_k$ of the map. The results of this computation are presented in Fig. 4, for orders $k = 4$, $k = 6$, and $k = 8$, in the region $(x_1, x_2) \in [-1, 1] \times [-1, 1]$, and show that $T_k^{\rm 2D}(F_2^{\rm 2D})$ is a good approximation of a symplectic map for $k \geq 6$, since $D_k \lesssim 10^{-6}$ for a large portion ($\gtrsim 77$ %) of variable values. As expected, the larger the order k, the closer the map $T_k^{\rm 2D}(F_2^{\rm 2D})$ numerically approaches the symplectic condition.

In order to check whether the controlled map $T_k^{\rm 2D}(F_2^{\rm 2D})$ with $k \geq 4$ increases the DA of the flat beam, we use again the SALI to determine the nature of orbits in the (x_1, x_2) plane, keeping in mind that SALI tends to zero both for regular and chaotic orbits of 2D maps, but with time rates which allow the clear distinction between the two cases. In particular, many initial conditions are tracked for 10^4 iterations in the (x_1, x_2) plane, and colored according to their final $\log_{10}$SALI value, for the $T^{\rm 2D}$ [Fig. 5(a)], the $T_6^{\rm 2D}(F_2^{\rm 2D})$ [Fig. 5(b)], and the $T_8^{\rm 2D}(F_2^{\rm 2D})$ map. Orbits with SALI $\leq 10^{-10}$ are characterized as chaotic and are colored in blue, while the remaining ones are regular. Similarly to Fig. 2 white regions correspond to escaping orbits. This distinction is based on the theoretical prediction that for regular orbits SALI $\propto 1/n^2 = 10^{-8}$ at

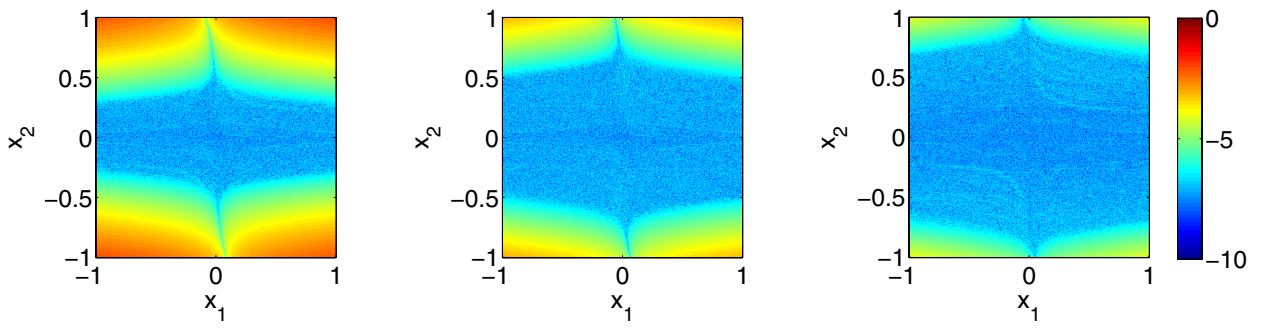

(a) (b) (c)

Fig. 4. Plot of $\log_{10} D_k$, where D_k is the norm of matrix $A_k^T J A_k - J$, and A_k is the Jacobian of the controlled map $T_k^{2D}(F_2^{2D})$, for 16 000 uniformly distributed values in the square $(x_1, x_2) \in [-1, 1] \times [-1, 1]$, for (a) $k = 4$, (b) $k = 6$, and (c) $k = 8$. The percentages of orbits with $\log_{10} D_k < -6$ are 53%, 77%, and 94% respectively for $k = 2$, 4, and 6. The color scale corresponds to the value of $\log_{10} D_k$; the smaller the value of $\log_{10} D_k$ is (blue region), the closer the map is to a symplectic one.

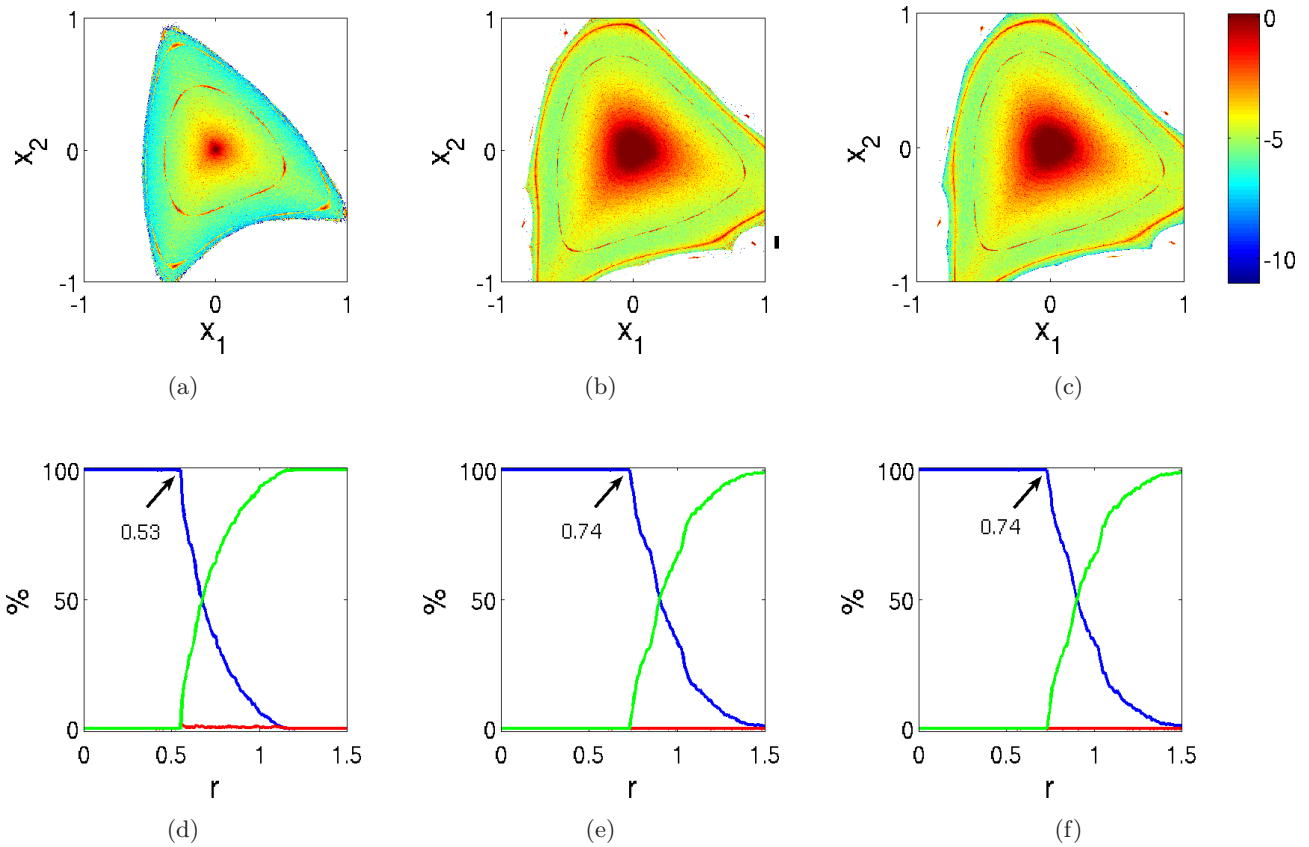

(a) (b) (c)

(d) (e) (f)

Fig. 5. (Upper row) Regions of different SALI values on the (x_1, x_2) plane of (a) the uncontrolled 2D map (14), (b) the $T_6^{2D}(F_2^{2D})$ controlled map, and (c) the $T_8^{2D}(F_2^{2D})$ controlled map. 16 000 uniformly distributed initial conditions in the square $(x_1, x_2) \in [-1, 1] \times [-1, 1]$ are followed for 10^4 iterations, and they are colored according to their final $\log_{10}$ SALI value. The white colored regions correspond to orbits that escape in less than 10^4 iterations. (Lower row) The percentages of regular (blue curves), chaotic (red curves), and escaping (green curves) orbits after $n = 10^4$ iterations of the maps of the upper row, in a circle centered at $x_1 = x_2 = 0$, as a function of its radius r. The largest radii at which the percentage of regular orbits is 100%, are marked in panels (d)–(f). Panels in the same columns correspond to the same map.

$n = 10^4$. In Figs. 5(d)–5(f) the percentages of regular (blue curves), chaotic (red curves), and escaping (green curves) orbits of these three maps are plotted as a function of the radius r of a circle centered at the origin $x_1 = x_2 = 0$.

In all models the number of chaotic orbits is practically negligible, which means that orbits are either regular or escaping. The two controlled maps succeed to increase the DA of the beam, because the domain of nonescaping orbits increases [Figs. 5(a)–5(c)]. Although this domain does not have a cyclical shape, the radius of the largest cycle containing only regular orbits increases from $r \approx 0.53$ for the uncontrolled map T^{2D} (14), to $r \approx 0.74$ for both controlled maps $T_6^{2D}(F_2^{2D})$ and $T_8^{2D}(F_2^{2D})$. Since both controlled maps give essentially the same results, we conclude that the sixth order truncation of the controlled map is sufficient for controlling the flat beam.

6. Summary and Discussion

In this paper, the results of the application of control theory to a simple 4D accelerator map [Boreux *et al.*, 2012], are being extended by using simplified versions of the control maps. In the first case, the momentum dependence of the control term is artificially removed, so as the control map is a function of the spatial coordinates and thus resembles the magnetic vector potential of a multipole magnet. In addition, this control map is symplectic by construction in contrast to the original one, thus avoiding the associated problems of having to choose an appropriate order of truncation in the Lie representation, for which the map satisfies numerically the symplectic condition. The efficiency of the simplified control map is remarkable, not only achieving the increase of the DA, but also shows a better performance as compared to the complete control map. The remaining important issue regarding the possibility to approximate in practice this magnetic field by a multipole magnet is still open, and will be addressed in a future study. In this respect, and based on the knowledge that control theory can be efficiently used to increase the DA of a toy model, the studies can be extended by investigating the possibility of imposing a control map with the functional form similar to Eq. (11), and compute the associated multipole coefficients which achieve the best increase in the DA.

In the second case, the same theory is applied to a 2D version of the map, modeling flat beams, as it is the case in electron and positron low emittance rings (i.e. with small beam sizes), where the vertical beam size is several orders of magnitude smaller than the horizontal one and thus the dynamic studies can be restricted to that plane. This 2D control map presents the same characteristics as the original map, i.e. increase of the DA, for a truncation order equal to six.

In all our studies, the SALI indicator was mainly used for showing the improvement of control in the DA. In future work, we plan to apply the frequency map analysis method (e.g. see [Laskar, 1999] and references therein) in this map in order to understand the dynamical details of this improvement with respect to resonance excitation and diffusion.

Acknowledgments

Numerical simulations were made on the local computing resources (CLUSTER URBM–SYSDYN) at the University of Namur (FUNDP, Belgium). Ch. Skokos was partly supported by the European research project "Complex Matter", funded by the GSRT of the Ministry Education of Greece under the ERA-Network Complexity Program. Ch. Skokos would like to thank J. Laskar for useful discussions and suggestions on the application of chaos control theory to accelerator models.

References

Boreux, J., Carletti, T., Skokos, Ch. & Vittot, M. [2012] "Hamiltonian control used to improve the beam stability in particle accelerator models," *Commun. Nonlin. Sci. Numer. Simulat.* **17**, 1725–1738.

Bourbaki, N. [1972] *Eléments de Mathématiques*: *Groupes et Algèbres de Lie* (Hermann Ed. Paris).

Bountis, T. & Tompaidis, S. [1991] *Future Problems in Nonlinear Particle Accelerators*, eds. Turchetti, G. & Scandale, W. (World Scientific, Singapore), p. 112.

Bountis, T. & Skokos, Ch. [2006a] "Application of the SALI chaos detection method to accelerator mappings," *Nucl. Instr. Meth. Phys. Res. — Sect. A* **561**, 173–179.

Bountis, T. & Skokos, Ch. [2006b] "Space charges can significantly affect the dynamics of accelerator maps," *Phys. Lett. A* **358**, 126–133.

Chandre, C., Vittot, M., Elskens, Y., Ciraolo, G. & Pettini, M. [2005] "Controlling chaos in area-preserving maps," *Physica D* **208**, 131–146.

Forest, E. [1998] *Beam Dynamics, A New Attitude and Framework* (Harwood Academic, Chur, Switzerland).

Laskar, J. [1999] "Introduction to frequency map analysis," *Proc. 3DHAM95 NATO Advanced Institute*, ed. Simoó, C. (SAgaro, June 1995).

Skokos, Ch. [2001] "Alignment indices: A new, simple method for determining the ordered or chaotic nature of orbits," *J. Phys. A* **34**, 10029–10043.

Skokos, Ch., Antonopoulos, C., Bountis, T. & Vrahatis, M. N. [2003] "How does the Smaller Alignment Index (SALI) distinguish order from chaos?" *Prog. Theor. Phys. Supp.* **150**, 439–443.

Skokos, Ch., Antonopoulos, Ch., Bountis, T. & Vrahatis, M. N. [2004] "Detecting order and chaos in Hamiltonian systems by the SALI method," *J. Phys. A* **37**, 6269–6284.

Skokos, Ch., Bountis, T. & Antonopoulos, Ch. [2007] "Geometrical properties of local dynamics in Hamiltonian systems: The Generalized Alignment Index (GALI) method," *Physica D* **231**, 30–54.

Vittot, M. [2004] "Perturbation theory and control in classical or quantum mechanics by an inversion formula," *J. Phys. A* **37**, 6337.

Vrahatis, M. N., Isliker, H. & Bountis, T. C. [1997] "Structure and breakdown of invariant tori in a 4-D mapping model of accelerator dynamics," *Int. J. Bifurcation and Chaos* **7**, 2707.

Widemann, H. [2007] *Particle Accelerator Physics* (Springer Verlag Ed., NY).